J Polym Res (2013) 20:272
DOI 10.1007/s10965-013-0272-8

ORIGINAL PAPER

Self-assembled nanostructure of polybenzoxazine resins from reaction-induced microphase separation with poly(styrene-*b*-4-vinylpyridine) copolymer

Wei-Cheng Chu · Jheng-Guang Li · Chih-Feng Wang · Kwang-Un Jeong · Shiao-Wei Kuo

Received: 3 June 2013 / Accepted: 9 September 2013

Abstract In this study, we synthesized the diblock copolymer poly(styrene-*b*-4-vinylpyridine) through nitroxide-mediated radical polymerization and then blended it with the monomer (3-phenyl-3,4-dihydro-2*H*-1,3-benzoxazin-6-yl)methanol (PA-OH). Fourier transform infrared (FTIR) spectroscopy revealed evidence for intermolecular hydrogen bonding between the pyridyl groups of P4VP and the OH group of PA-OH. Thermal curing resulted in the block copolymer being incorporated into the polybenzoxazine resin, forming a nanostructure through a mechanism involving reaction-induced microphase separation, as evidenced using transmission electron microscopy (TEM) and small-angle X-ray scattering (SAXS). This approach also provided a variety of composition-dependent nanostructures, including disordered spherical, wormlike, and cylindrical structures through the intriguing balance between the contents of the polybenzoxazine and the diblock copolymer.

Keywords Polybenzoxazine · Self-assembly · Hydrogen bonding · Block copolymer

W.-C. Chu · J.-G. Li · S.-W. Kuo (✉)
Department of Materials and Optoelectronic Science, Center for Nanoscience and Nanotechnology, National Sun Yat-Sen University, Kaohsiung 804, Taiwan
e-mail: kuosw@mail.nsysu.edu.tw

C.-F. Wang
Department of Materials Science and Engineering, I-Shou University, 84041 Kaohsiung, Taiwan

K.-U. Jeong
Department of Polymer-Nano Science and Technology, Chonbuk National University, Jeonju 561-756, Korea

Published online: 06 October 2013

Introduction

Recently, the development of polybenzoxazine-based phenolic resins has received much attention because these resins combine characteristics found in traditional phenolic resins (e.g., high thermal stability, flame retardance) with properties that are typically not (e.g., low water absorption, no curing agents or harsh catalysts needed for polymerization, good dielectric properties, low surface free energies) [1–9]. In general, benzoxazine monomers, which are intriguing heterocyclic (oxazine-containing) compounds, have attracted considerable interest owing to their uses as cyclic monomers. They are synthesized through the reaction of a primary amine with phenol and formaldehyde; they can be polymerized through ring-opening polymerization in the absence of a catalyst, releasing no by-product in the process [1].

The self-assembly of amphiphilic block copolymers into different thermoset polymers (e.g., phenolic and epoxy resins) has been used widely to prepare long-range-ordered nanostructures [10–18]. For example, Ikkala and Ruokolainen et al. prepared long-range-ordered mesoporous phenolic resins from the diblock copolymers poly(isoprene-*b*-2-vinylpyridine) (PI-*b*-P2VP) and poly(styrene-*b*-4-vinylpyridine) (PS-*b*-P4VP) as templates, with hexamethylenetetramine (HMTA) as the curing agent [19–21]. Zheng et al. also reported the formation of long-range-ordered nanostructures in phenolic thermosets after curing novolac and the diblock copolymer poly(styrene-*b*-ethylene oxide) (PS-*b*-PEO) with HMTA [22]. Long-range-ordered nanostructures can be formed after mixing uncured phenolic resins with block copolymers featuring a block that forms sufficiently strong hydrogen bonds with the phenolic OH groups such that curing of the phenolic resin will preserve the self-assembled structure without undergoing macroscopic phase separation [20, 23–26]. As a result, varying the intermolecular interaction strength of polybenzoxazine with a block copolymer template

to form sufficiently strong hydrogen bonds appeared to be a potential route toward the preparation of long-range-ordered nanostructures based on polybenzoxazine [27, 28].

In our previous study, we blended the diblock copolymer poly(ethylene oxide-*b*-ε-caprolactone) (PEO-*b*-PCL) with the monomer (3-phenyl-3,4-dihydro-2*H*-1,3-benzoxazin-6-yl)methanol (PA-OH) [29–31]. Thermal curing resulted in the block copolymer being incorporated into the polybenzoxazine resin, forming cylindrical, wormlike, and disordered spherical nanostructures through a mechanism involving reaction-induced microphase separation, as evidenced using transmission electron microscopy (TEM) and small-angle X-ray scattering (SAXS). Intermolecular hydrogen-bonding interactions between the hydroxyl groups of PA-OH and the ether groups of PEO as well as the carbonyl groups of PCL made the system complicated [32–34]. In this study, we changed the template to the more common diblock copolymer PS-*b*-P4VP, synthesized through nitroxide-mediated radical polymerization (NMRP). We expected the free OH group of PA-OH to form strong intermolecular hydrogen bonds with the pyridyl groups of the P4VP block of the copolymer, both before and after the curing reaction (Scheme 1), possibly forming a variety of composition-dependent nanostructures (e.g., cylindrical, wormlike, spherical). Herein, we describe the phase behavior and hydrogen-bonding interactions of polybenzoxazine nanostructures, which we investigated using differential scanning calorimetry (DSC), Fourier transform infrared (FTIR) spectroscopy, SAXS, and TEM.

Experimental

Materials

Styrene and 4-vinylpyridine (distilled from finely ground CaH_2 prior to use) were purchased from Aldrich, as were paraformaldehyde, aniline, acryloyl chloride, and 4-hydroxybenzyl alcohol. The following chemicals and solvents were used as received: benzoyl peroxide (BPO, >97 %, Fluka), 2,2,6,6-tetramethylpiperidinooxy (TEMPO, 98 %, ACROS), tetrahydrofuran (THF, HPLC grade, TEDIA),

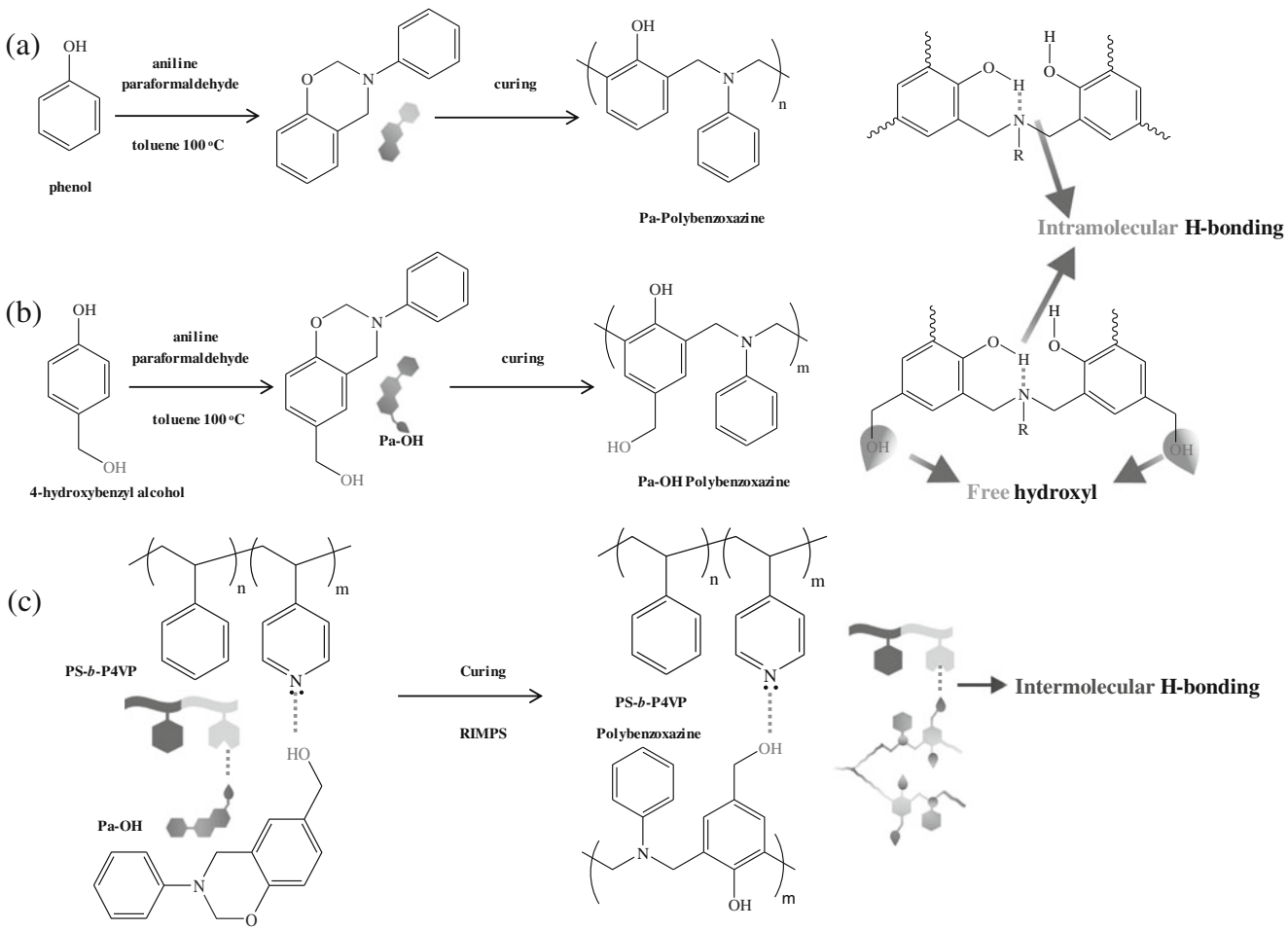

Scheme 1 Chemical reactions and corresponding cross-linked structures of **a** PA- and **b** PA-OH-type polybenzoxazines. **c** Inter-association between PA-OH-type polybenzoxazine and PS-*b*-P4VP (*brown* PS, *orange* P4VP)

methanol (MeOH, HPLC grade, TEDIA), and diethyl ether (Et_2O, HPLC grade, TEDIA). The diblock copolymers 1-hydroxy-2-phenyl-2-(2′,2′,6′,6′-tetramethyl-1-piperidinyloxy)ethane (TEMPO-OH) [35, 36] and poly(styrene-*b*-4-vinylpyridine) (PS_{198}-*b*-$P4VP_{221}$; M_n=44,000 g/mol; PDI=1.19; f_{PS}^{v}=0.39) were prepared as described previously [37]. Reactions were performed in glassware under a static atmosphere of Ar.

(3-Phenyl-3,4-dihydro-2*H*-1,3-benzoxazin-6-yl)methanol (PA-OH) [29]

4-Hydroxybenzyl alcohol (4.96 g, 40.0 mmol) and paraformaldehyde (2.40 g, 80.0 mmol) were placed in a 100-mL three-neck flask cooled in an ice bath and then a solution of aniline (3.72 g, 40.0 mmol) in toluene (60 mL) was added. The mixture was heated under reflux at 100 °C for 8 h. After cooling to room temperature, the solid residue was filtered off and recrystallized (toluene) to afford pale yellow crystals (80 %). ^{1}H NMR ($CDCl_3$, ppm): 4.55 (s, ArCH_2OH), 4.63 (s, CCH_2N), 5.36 (s, NCH_2O), 6.77–7.40 (m, Ar). ^{13}C NMR ($CDCl_3$, ppm): 50.48 (CCH_2N), 64.86 (ArCH_2OH), 79.45 (NCH_2O). IR (KBr, cm^{-1}): 3,350 (OH stretching), 947 (out-of-plane CH bending).

Nanostructured polybenzoxazines

PA-OH and PS-*b*-P4VP were dissolved in THF at different ratios until the solutions were homogenous. The solvent was evaporated slowly at room temperature and then the samples were vacuum-dried at 30 °C overnight. Curing of the samples was performed using the following temperature profile: 110 °C for 6 h, 160 °C for 4 h, 180 °C for 4 h, 200 °C for 2 h, 220 °C for 1 h, and 240 °C for 0.5 h.

Characterization

^{1}H NMR spectra were recorded at room temperature using a Bruker AM 500 (500 MHz) spectrometer, with $CDCl_3$ as the solvent and the signal of residual $CHCl_3$ as the internal standard. Molecular weights and molecular weight distributions were determined through gel permeation chromatography (GPC) using a Waters 510 HPLC system equipped with a 410 differential refractometer and three Ultrastyragel columns (100, 500, and 10^3 Å) connected in series; DMF was the eluent (flow rate 1.0 mL/min). DSC was performed using a TA-Q20 instrument operated at a scan rate of 20 °C/min over a temperature range from 0 to 250 °C under a N_2 atmosphere. FTIR spectra of the samples were recorded using the conventional KBr disk method. The spectra were recorded using a Bruker Tensor 27 FTIR spectrophotometer. SAXS was performed using a Nanostar U SAXS system (Bruker, Germany) and Cu Kα radiation (40 kV, 35 mA). The *d* spacings were calculated using the formula $d = 2\pi/q$. TEM was conducted using a JEOL 3010 microscope (Japan) operated at 200 kV. Ultrathin sections of the samples were prepared using a Leica Ultracut S microtome equipped with a diamond knife; slices (thickness ca. 700 Å) were cut at room temperature. The ultrathin sections were placed onto Cu grids coated with carbon-supporting films; polybenzoxazine/P4VP blends were subsequently stained through exposure to I_2 vapor (I_2 was the preferred staining agent because P4VP and polybenzoxazine/P4VP domains appeared dark and PS domains, bright, in the micrographs).

Results and discussion

PA-OH/block copolymer blend analyses

DSC is a convenient method for determining the miscibility of polymer blends. Figure 1 displays the conventional second-run DSC thermograms, recorded at a heating rate of 20 °C/min, of PA-OH/PS-*b*-P4VP blends of various compositions. PA-OH exhibited a melting temperature near 90 °C, similar to those of other benzoxazine monomers [1], as well as a glass transition temperature (T_g) near 4 °C. Low molecular weight compounds presenting OH groups typically feature single-T_g behavior during the second heating scan [38–41]. The PS-*b*-P4VP diblock copolymer (T_g=108.2 and 153.3 °C) exhibited

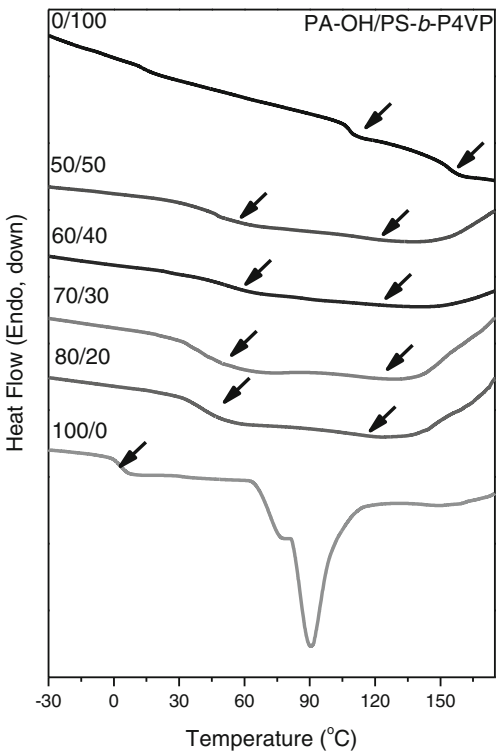

Fig. 1 DSC thermograms of Pa-OH/PS-*b*-P4VP blends of various compositions

two glass transitions, indicating chemical incompatibility between the constituent blocks that might lead to microphase separation. The lower-temperature glass transition corresponds to the PS block; the higher, to the P4VP block. In addition, the value of T_g of the PS block in the diblock copolymers was higher than that of PS homopolymer, presumably because of hard confinement and the presence of fewer chain ends [42]. We suspect that the PS block segment in the diblock copolymer existed in the form of a nanostructure with more-compact packing, resulting in a smaller free volume and higher value of T_g. Two glass transitions appeared for the PA-OH/PS-*b*-P4VP blends. We assign the higher value of T_g (at ca. 108 °C) to the PS-dominant phase, which had phase-separated from the mixed and miscible phase of PA-OH and P4VP. The lower value of T_g arose from the miscible, hydrogen-bonded PA-OH and P4VP phase. Thus, the blends formed stable mixed phases over a wide range of PA-OH volume fractions. In addition, we found a curing exothermic peak of greater than 150 °C for all of the blend systems, implying that the PA-OH remained thermally activated for ring-opening polymerization and could form cross-linked structures even after blending with the diblock copolymer PS-*b*-P4VP.

Next, we used FTIR spectroscopy to provide evidence for hydrogen-bonding interactions within the PA-OH/P4VP matrix. The OH stretching region in the room temperature FTIR spectra of the blends of the diblock copolymer PS-*b*-P4VP and PA-OH, cast from THF solutions, was sensitive to the existence of hydrogen bonds (Fig. 2a). The spectrum of PA-OH featured two major unresolved bands in the OH stretching region, corresponding to the free OH groups at 3,525 cm^{-1} and a broad band centered at 3,400 cm^{-1} arising from absorption of hydrogen-bonded OH groups (self-association). The intensity of the signal for the free OH groups decreased gradually upon increasing the content of the diblock copolymer PS-*b*-P4VP, as we had expected. This signal for free OH groups disappeared essentially when the content of PS-*b*-P4VP reached 50 wt.%, indicating that more of the OH groups formed hydrogen bonds with pyridyl groups as the concentration of the pyridyl groups increased. Meanwhile, the peak frequency of the broad band shifted to lower wavenumber upon increasing the PS-*b*-P4VP content, reflecting a distribution of hydrogen bonds (i.e., both OH···OH interactions between PA-OH units and OH···pyridyl interactions between PA-OH and P4VP units). This feature also revealed that the interaction between the OH group of PA-OH and the pyridyl units of P4VP became the dominant one in blends that were rich in PS-*b*-P4VP. Therefore, we assign the band at 3,200 cm^{-1} to the OH groups of PA-OH hydrogen-bonded to pyridyl units of the P4VP block. We used the frequency difference between the signals of the hydrogen-bonded and free OH groups ($\Delta\nu$) to roughly estimate the average strength of hydrogen bonding [43]. In this respect, the hydrogen bonds formed between the OH groups of PA-OH and the pyridyl units of P4VP in the diblock copolymer ($\Delta\nu$=325 cm^{-1}) were stronger than those between pairs of PA-OH moieties ($\Delta\nu$= 125 cm^{-1}).

In addition to the OH stretching region, some of the characteristic modes of the pyridyl rings are also sensitive to the presence of hydrogen bonds. For example, the signals of P4VP at 1,590, 1,050, 993, and 625 cm^{-1} shifted to 1,600, 1,067, 1,011, and 634 cm^{-1}, respectively, after hydrogen

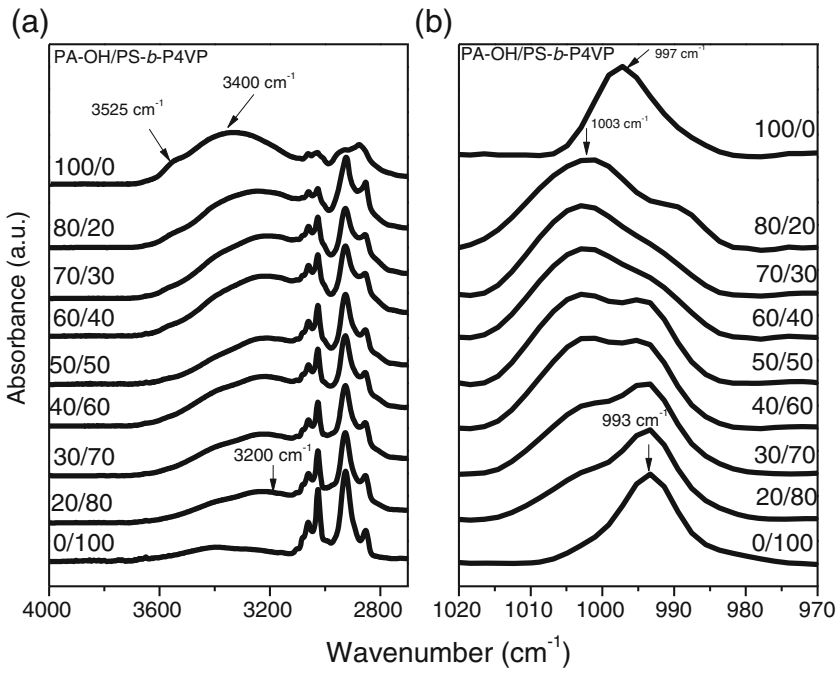

Fig. 2 Room temperature FTIR spectra of PA-OH/PS-*b*-P4VP blends, displaying the **a** OH stretching and **b** pyridyl regions

Table 1 Curve fitting of fraction of hydrogen-bonding results of PA-OH/PS-*b*-P4VP at room temperature

PA-OH/PS-*b*-P4VP	Free pyridine ring			H-bonded pyridine ring			f_b (%)
	ν (cm^{-1})	$W_{1/2'}$	A_f (%)	ν (cm^{-1})	$W_{1/2'}$	A_b (%)	
20:80	993	10	63.4	1,003	11	37.6	37.6
30:70	993	10	51.6	1,003	11	48.4	48.4
40:60	993	10	34.9	1,003	11	65.1	65.1
50:50	993	10	31.5	1,003	11	68.5	68.5
60:40	993	10	26.7	1,003	11	73.3	73.3
70:30	993	9	21.8	1,003	11	78.2	78.2
80:20	993	9	11.5	1,002	11	88.5	88.5

bonding with the carboxylic acid groups of poly(ethylene-*co*-methacrylic acid) [44]. Unfortunately, it was difficult for us to analyze the band at 1,590 cm^{-1} for P4VP because of overlap with the band at 1,600 cm^{-1} from PA-OH. Therefore, we could use only the band at 993 cm^{-1} to analyze the hydrogen-bonding interactions between the OH group of PA-OH and the pyridyl groups of P4VP. Figure 2b presents room temperature FTIR spectra in the range 970–1,020 cm^{-1} for the blends of PA-OH and PS-*b*-P4VP. The P4VP block provided a characteristic band at 993 cm^{-1}, corresponding to the free pyridyl rings; pure PA-OH provided a band at 997 cm^{-1}. These two bands were well resolved, without overlapping. Upon blending of PS-*b*-P4VP and PA-OH, a new band appeared at 1,003 cm^{-1}, which we assign to the hydrogen-bonded pyridyl rings of the P4VP block. The FTIR spectra of all of the blend systems revealed the existence of hydrogen bonding between the pyridyl and OH groups, but it was difficult to quantify the degree of hydrogen bonding because of the presence of three bands in this region. As a result, we performed a digital subtraction of the signal for pure PA-OH at 997 cm^{-1} on the basis of the weight fraction of PS-*b*-P4VP in these blends [45, 46]. All of the signals for the pyridyl groups split into two bands that fit well to the Gaussian function. Table 1 summarizes the results from curve fitting; the fraction of hydrogen-bonded pyridyl rings increased upon increasing the PA-OH content in this blend system, similar to our previously reported findings for phenolic/P4VP and PVPh/P4VP blends [45, 46].

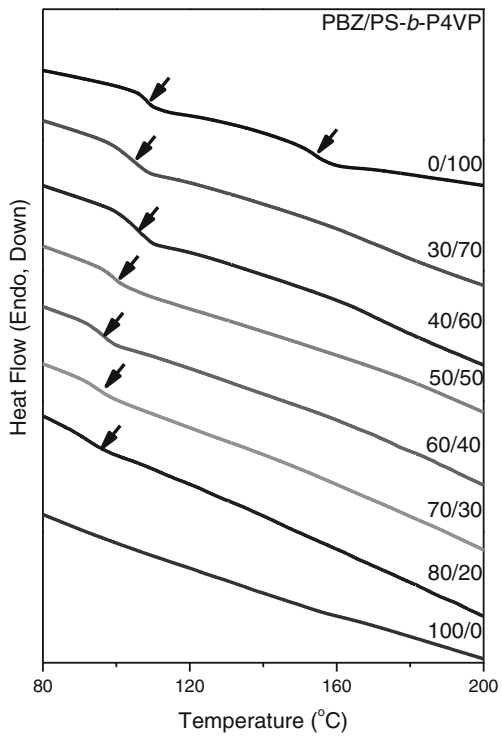

Fig. 3 DSC thermograms of PA-OH-type polybenzoxazine/PS-*b*-P4VP blends of various compositions

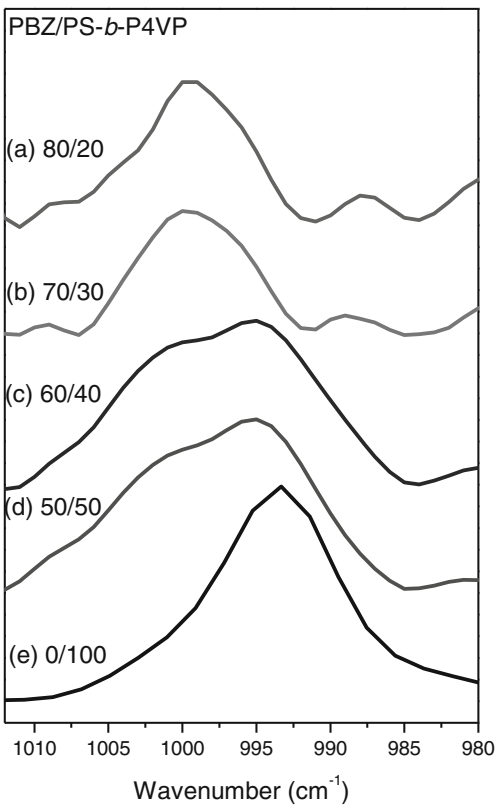

Fig. 4 Room temperature FTIR spectra of PA-OH-type polybenzoxazine/PS-*b*-P4VP blends

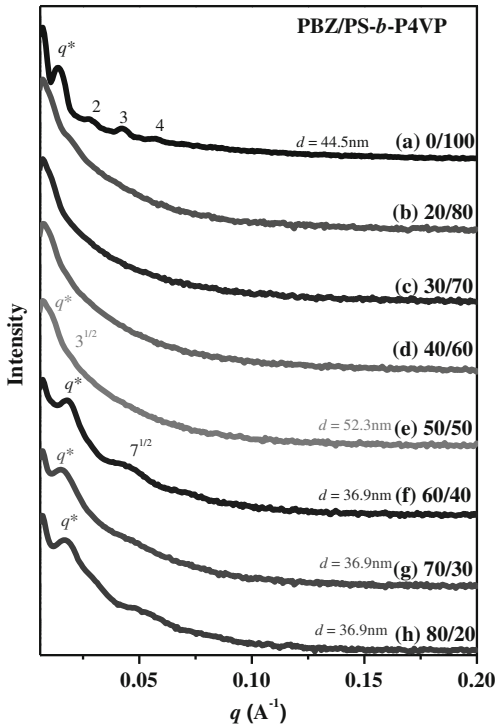

Fig. 5 Profiles of SAXS intensities of polybenzoxazine/PS-*b*-P4VP blends of various compositions

Analyses of polybenzoxazine/block copolymer blends

We incorporated the diblock copolymer PS-*b*-P4VP into polybenzoxazine to prepare nanostructures in the thermoset polymer. Prior to thermal curing, all of our binary mixtures of the benzoxazine PA-OH and the diblock copolymer PS-*b*-P4VP were homogenous and transparent. After thermal curing, the polybenzoxazines remained homogenous and transparent, but became dark red in color, suggesting that macrophase separation did not occur. Nevertheless, reaction-induced microphase separation cannot be explained merely in terms of sample clarity. Therefore, we investigated the thermal behavior of the polybenzoxazine/PS-*b*-P4VP blends prior to pyrolysis. Figure 3 displays conventional second-run DSC thermograms of the pure PS-*b*-P4VP block copolymers and the polybenzoxazine/PS-*b*-P4VP blends. For pure PS-*b*-P4VP, the glass transitions of the PS and P4VP blocks appeared clearly at 108 and 153 °C, respectively, as mentioned previously. In the DSC traces of the blends, however, we observed the glass transition only of the PS segment; the DSC curves of polybenzoxazine/P4VP phases became very broad. This behavior is often observed when P4VP is blended with nanoparticles or thermoset polymers; it provides evidence for the loss of mobility of the P4VP chains upon blending with the polybenzoxazine matrix [47].

Figure 4 presents room temperature FTIR spectra of the polybenzoxazine/PS-*b*-P4VP blends in the range 980–1,020 cm^{-1}. The free pyridyl rings of the P4VP block provided a characteristic band at 993 cm^{-1}. Upon blending of PS-*b*-P4VP with the PA-OH-type polybenzoxazine, a new appeared band at 1,001 cm^{-1}, which we assign to the hydrogen-bonded pyridyl rings of the P4VP block. Similar to the spectra of the PA-OH/PS-*b*-P4VP blend systems, the fraction of hydrogen-bonded pyridyl rings increased upon increasing the content of PA-OH-type polybenzoxazine in this blend system, but the absorption shift and fraction of hydrogen-bonded pyridyl units were both less than those in the PA-OH/PS-*b*-P4VP blends. This behavior is reasonable because the P4VP blocks blended with the thermoset polymer would undergo a loss of mobility relative to those chains blended with the PA-OH monomer.

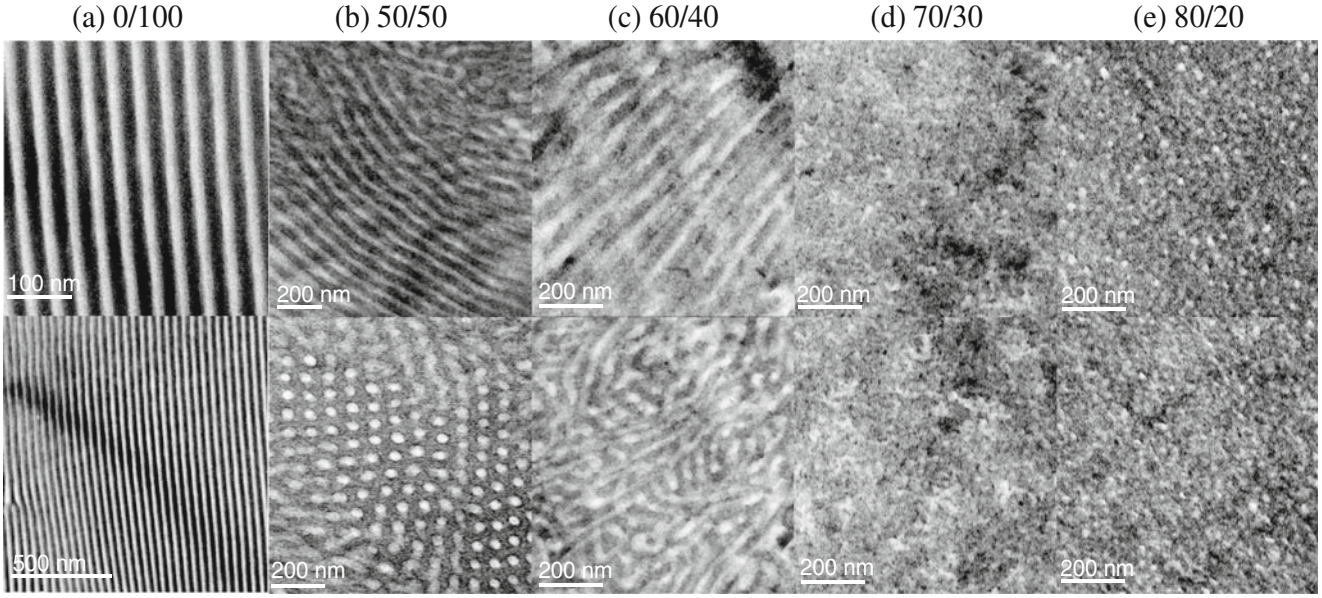

Fig. 6 Transmission electron micrographs of polybenzoxazine/PS-*b*-P4VP blends at compositions of **a** 0:100, **b** 50:50, **c** 60:40, **d** 70:30, and **e** 80:20

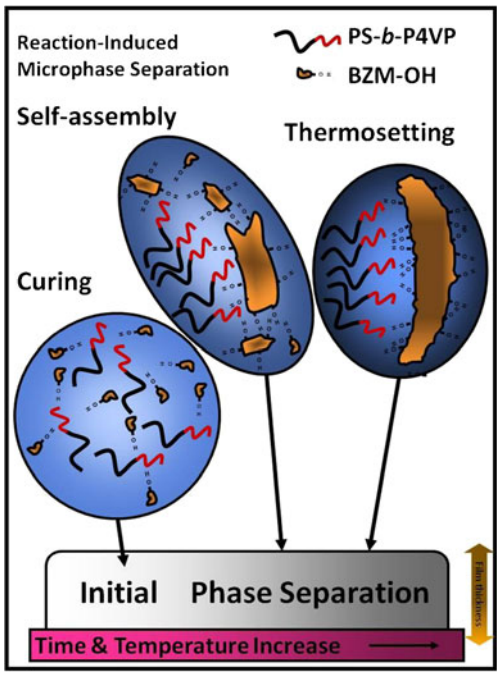

Scheme 2 Possible mechanism for the formation of self-assembled nanostructures from polybenzoxazine/PS-*b*-P4VP blends

Nanostructures of polybenzoxazine/PS-b-P4VP blends

We recorded SAXS profiles of the polybenzoxazine resins templated by the block copolymer PS-*b*-P4VP at room temperature to confirm the self-organized morphologies (Fig. 5). SAXS analysis revealed a lamellar micro-domain structure for pure PS-*b*-P4VP, judging from the scattering maxima at relative positions of 1:2:3:4. The set of SAXS peaks located at the positions of multiples of q^* of 0.014 $Å^{-1}$ indicate a lamellar phase having a long period of 44.8 nm, extracted from the first peak position ($2\pi/q$). The TEM image in Fig. 6a reveals that the pure PS-*b*-P4VP diblock copolymer exhibited an alternating lamellar morphology and long-range-ordered pattern having a lamellar period of approximately 40 nm, consistent with the SAXS data in Fig. 5a. At relatively low polybenzoxazine contents (<40 wt.%), the SAXS profiles in Fig. 5b–d feature broad peaks corresponding to short-range-ordered or disordered polybenzoxazine resins. This behavior is similar to that in many previously reported thermoset/block copolymer blends [26]; it suggests that insufficient polybenzoxazine resin was present relative to the templating PS-*b*-P4VP block copolymer. A hexagonally packed cylinder structure appeared, on the basis of SAXS analysis, at a polybenzoxazine content of 50 wt.% (Fig. 5e); the maximum intensity appeared at a value of q^* of approximately 0.012 $Å^{-1}$ (d=52.3 nm) with second-order reflections at $3^{1/2}q^*$ (see inset). This result is consistent with the TEM image in Fig. 6b. After I_2 staining, the polybenzoxazine and P4VP microdomains appeared dark and the PS microdomains appeared light. The average microdomain radius and the distance between cylinders, as measured from the TEM micrographs, were both approximately 50 nm, consistent with the SAXS data. To the best of our knowledge, this system is the first reported example of an ordered self-assembled nanostructure based on a polybenzoxazine resin. When the polybenzoxazine content was 60 wt.%, the SAXS pattern (Fig. 5f) featured only a single sharp peak at a value of q^* of approximately 0.017 $Å^{-1}$ (d= 36.9 nm) and another small peak near $7^{1/2}$, due to incomplete disordering of the hexagonal cylinders present in this blend. The TEM image in Fig. 6c reveals a worm-like structure for the polybenzoxazine/PS-*b*-P4VP=60:40 sample, similar to that of a previously reported phenolic/PS-*b*-P4VP=70:30 system [26]. Further increases in the polybenzoxazine content to 70 and 80 wt.% resulted in a broad intensity maximum at a value of q^* of 0.017 $Å^{-1}$ (d= 36.9 nm), with no other resolvable higher-order peaks (Fig. 5g, h). This behavior suggests a spherical (micelle) structure with short-range order, as confirmed in the TEM images in Fig. 6d, e. Again, this structure is similar to those

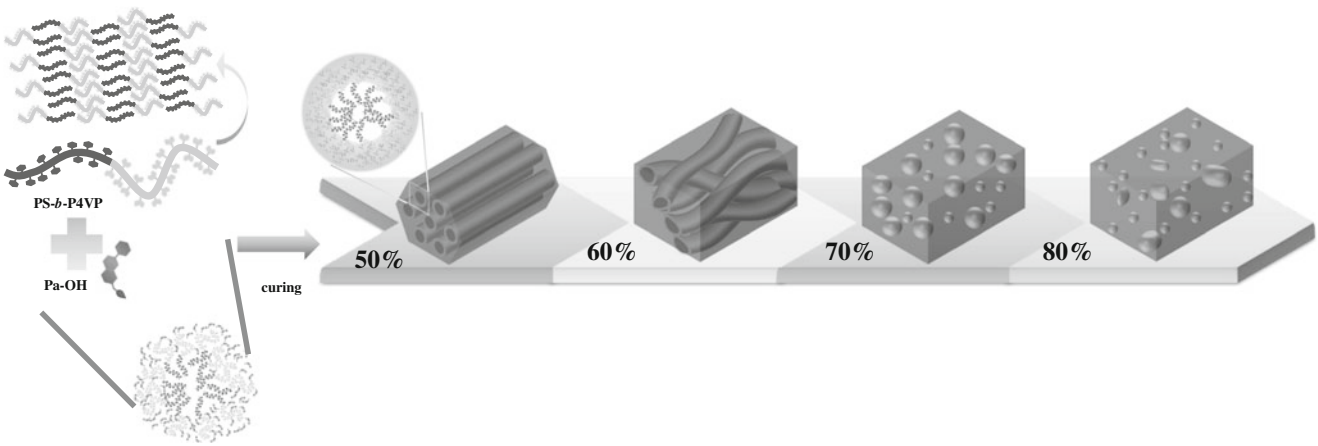

Scheme 3 Morphological changes in the self-assembled nanostructures of polybenzoxazines upon increasing the polybenzoxazine content

found in previous studies of phenolic/PS-*b*-P4VP=80:20 [26] and PBa-type polybenzoxazine/PS-*b*-PVPy=80:20 systems [27]. The formation of nanostructures in thermosets templated by amphiphilic block copolymers could occur through mechanisms involving reaction-induced microphase separation. Scheme 2 displays a possible mechanism for the self-assembly of nanostructures from polybenzoxazine/PS-*b*-P4VP blends. In the first step, the PA-OH precursor behaves as a selective solvent for the PS-*b*-P4VP diblock copolymer to form self-organized nanophase structures (e.g., micelles) prior to thermal curing; these nanostructures were locked in during the subsequent curing reaction (Scheme 2a). As a result, we observed two values of T_g for the PA-OH/PS-*b*-P4VP blends on the basis of Fig. 1. Prior to curing, the miscibility of PA-OH with P4VP resulted from the non-negligible contribution of the mixing entropy to the mixing free energy, because the molecular weight of the PA-OH monomer is quite low. During thermal curing, however, the miscibility of the PA-OH-based polybenzoxazine with P4VP resulted from the formation of intermolecular hydrogen bonds between the pyridyl groups of P4VP and the free OH groups of the polybenzoxazine (Scheme 2b). After thermal curing, the reaction-induced microphase separation was complete; the P4VP segments were presumably miscible with the PA-OH-based polybenzoxazine, but the PS segments were excluded from this miscible domain (Scheme 2c). As a result, the *d* spacing of first peak decreased upon increasing the polybenzoxazine content, because the dissolving of the polybenzoxazine into the P4VP segments induced a loss of mobility for the P4VP chains and decreased the distance between the nanostructures in this thermoset/block copolymer blend. The whole mechanism of PA-OH-type polybenzoxazine blending with PS-*b*-P4VP is summarized in Scheme 3.

Conclusions

We have employed DSC, TEM, SAXS, and FTIR spectroscopy to investigate the miscibility, phase behavior, and hydrogen bonding within polybenzoxazine/PS-*b*-P4VP blends. DSC and FTIR spectroscopy provided evidence for the pyridyl groups of P4VP being hydrogen bond acceptors for the OH groups of the PA-OH-type polybenzoxazine. SAXS and TEM analyses indicated that different compositions of polybenzoxazine/PS-*b*-P4VP blends resulted in different microphase-separated structures such as disordered spherical, wormlike, and cylindrical structures, mediated through hydrogen-bonding interactions.

Acknowledgment This work was supported financially by the National Science Council, Taiwan, Republic of China, under Contract No. NSC 100-2221-E-110-029-MY3 and NSC 100-2628-E-110-001.

References

1. Ishida H (2011) In: Ishida H, Agag T (eds) Handbook of polybenzoxazine resins. Elsevier, Amsterdam, Chap 1, p 1
2. Wang CF, Su YC, Kuo SW, Huang CF, Sheen YC, Chang FC (2006) Angew Chem Int Ed 45:2248–2251
3. Kuo SW, Wu YC, Wang CF, Jeong KU (2009) J Phys Chem C 113: 20666–20673
4. Wang CF, Chiou SF, Ko FH, Chen JK, Chou CT, Huang CF, Kuo SW, Chang FC (2007) Langmuir 23:5868–5871
5. Wang CF, Chang FC, Kuo SW (2011) In: Ishida H, Agag T (eds) Handbook of polybenzoxazine resins. Elsevier, Amsterdam, Chap 33, pp 579–591
6. Ning X, Ishida H (1994) J Polym Sci A Polym Chem 32:1121–1129
7. Cui HW, Kuo SW (2013) J Polym Res 20:114
8. Wang CF, Wang TF, Liao CS, Kuo SW, Lin HC (2011) J Phys Chem C 115:16495–16500
9. Kiskan B, Ghosh NN, Yagci Y (2010) Polym Int 60:167–177
10. Hillmyer MA, Lipic PM, Hajduk DA, Almdal K, Bates FS (1997) J Am Chem Soc 119:2749–2750
11. Guo Q, Thomann R, Gronski W (2002) Macromolecules 35:3133–3144
12. Meng F, Zheng S, Li H, Liang Q, Liu T (2006) Macromolecules 39: 5072–5079
13. Maiez-Tribut S, Pascault JP, Soule ER, Borrajo J, Williams RJJ (2007) Macromolecules 40:1268–1273
14. Xu Z, Zheng S (2007) Macromolecules 40:2548–2558
15. Ritzenthaler S, Court F, David I, Girard-Reydet E, Leibler I, Pascault JP (2002) Macromolecules 35:6245–6254
16. Fan W, Wang L, Zheng S (2009) Macromolecules 42:327–336
17. Meng F, Xu Z, Zheng S (2008) Macromolecules 41:1411–1420
18. Mijovic J, Shen M, Sy JW (2000) Macromolecules 33:5235–5244
19. Kosonen H, Ruokolainen J, Nyholm P, Ikkala O (2001) Polymer 42: 9481–9486
20. Kosonen H, Ruokolainen J, Nyholm P, Ikkala O (2001) Macromolecules 34:3046–3049
21. Valkama S, Nykanen A, Kosonen H, Ramani R, Tuomisto F, Engelhardt P, ten Brinke G, Ikkala O, Ruokolainen J (2007) Adv Funct Mater 17:183–190
22. Hu D, Xu Z, Zeng K, Zheng S (2010) Macromolecules 43:2960–2969
23. Liang C, Dai S (2006) J Am Chem Soc 128:5316–5317
24. Kosonen H, Ruokolainen J, Torkkeli M, Serimaa R, Nyholm P, Ikkala O (2002) Macromol Chem Phys 203:388–392
25. Kosonen H, Valkama S, Nykänen A, Torkkeli M, ten Brinke G, Ruokolainen J, Ikkala O (2006) Adv Mater 18:201–205
26. Su YC, Chen WC, Ou KL, Chang FC (2005) Polymer 46:3758–3766
27. Hu D, Zheng S (2010) Polymer 51:6346–6354
28. Li Y, Zheng S (2010) J Polym Sci B Polym Phys 48:1148–1159
29. Chu WC, Li JG, Kuo SW (2013) RSC Adv 3:6485–6498
30. Kudoh R, Sudo A, Endo T (2010) Macromolecules 43:1185–1187
31. Kiskan B, Koz B, Yagci Y (2009) J Polym Sci A Polym Chem 47: 6955–6961
32. Kiskan B, Yagci Y (2005) Polymer 46:11690–11697
33. Zheng S, Lu H, Guo Q (2004) Macromol Chem Phys 205:1547–1558
34. Ishida H, Lee YH (2001) J Polym Sci B Polym Phys 39:736–749
35. Chen SC, Kuo SW, Lu CH, Lee HF, Chang FC (2007) Polymer 48: 5059–5068
36. Lu CH, Huang CF, Kuo SW, Chang FC (2009) Macromolecules 42: 1067–1078
37. Lu CH, Wang JH, Chang FC, Kuo SW (2010) Macromol Chem Phys 211:1339–1347
38. Kuo SW (2008) J Polym Res 15:459–486
39. Kuo SW, Chan SC, Chang FC (2002) Polymer 43:3653–3660

40. Kuo SW, Lin HC, Huang WJ, Huang CF, Chang FC (2006) J Polym Sci Polym Phys 44:673–686
41. Huang KW, Tsai LW, Kuo SW (2009) Polymer 50:4876–4887
42. Chen SC, Kuo SW, Jeng US, Chang FC (2010) Macromolecules 43: 1083–1092
43. Coleman MM, Painter PC (2006) Miscible polymer blend: background and guide for calculations and design. DEStech, Lancaster, PA
44. Lee YJ, Painter PC, Coleman MM (1988) Macromolecules 21:954–960
45. Kuo SW, Lin CL, Chang FC (2002) Polymer 43:3943–3949
46. Kuo SW, Tung PH, Chang FC (2006) Macromolecules 39:9388–9395
47. Yeh SW, Wei KH, Sun YS, Jeng US, Liang KS (2005) Macromolecules 38:6559–6565